

Spin-state crossover and hyperfine interactions of ferric iron in MgSiO₃ perovskite

Han Hsu,¹ Peter Blaha,² Matteo Cococcioni,¹ and Renata M. Wentzcovitch¹

¹*Department of Chemical Engineering and Materials Science,*

University of Minnesota, Minneapolis, Minnesota, USA

²*Institute of Materials Chemistry, Vienna University of Technology,*

A-1060 Vienna, Getreidemarkt 9/165-TC, Austria

(Dated: October 10, 2018)

Abstract

Using density functional theory plus Hubbard U calculations, we show that the ground state of (Mg,Fe)(Si,Fe)O₃ perovskite, the major mineral phase in the Earth's lower mantle, has high-spin ferric iron ($S = 5/2$) at both dodecahedral (A) and octahedral (B) sites. With increasing pressure, the B-site iron undergoes a spin-state crossover to the low-spin state ($S = 1/2$) between 40 and 70 GPa, while the A-site iron remains in the high-spin state. This B-site spin-state crossover is accompanied by a noticeable volume reduction and an increase in quadrupole splitting, consistent with recent X-ray diffraction and Mössbauer spectroscopy measurements. The anomalous volume reduction leads to a significant softening in the bulk modulus during the crossover, suggesting a possible source of seismic-velocity anomalies in the lower mantle.

PACS numbers: 91.60.Pn, 76.80.+y, 91.60.Gf, 91.60.Fe

20 The total electron spin (S) of a transition-metal ion in a crystalline solid can change with
21 many factors, such as pressure, strain, or temperature, to name a few. This phenomenon,
22 known as spin-state crossover, is of great importance in spintronics, as it allows artificial
23 control of magnetic properties of materials, including coordination complexes with potential
24 for molecular switches [1]. Not as widely known, spin-state crossover also plays a crucial role
25 in geophysics. A well studied example is ferropericlase, $(\text{Mg,Fe})\text{O}$, the second most abundant
26 mineral (~ 20 vol%) in the the largest single region (~ 55 vol%) of the Earth's interior -
27 the lower mantle. With increasing pressure, ferrous iron (Fe^{2+}) in this mineral undergoes a
28 crossover from high-spin (HS) state, $S = 2$, to low-spin (LS) state, $S = 0$, in the pressure
29 range of 40-55 GPa [2–6]. The intermediate-spin (IS) state, $S = 1$, is not observed in
30 this mineral. The HS-LS crossover in ferropericlase directly affects the structural, elastic,
31 optical, and conducting properties of this mineral [6–11] and thus affects mantle properties.
32 [10, 12, 13].

33 In contrast, the spin-state crossover in iron-bearing magnesium silicate (MgSiO_3) per-
34 ovskite (Pv), the most abundant mineral (~ 75 vol%) in the lower mantle, has been a source
35 of controversy for two main reasons. One is the coexisting ferrous and ferric iron (Fe^{3+}) in
36 this mineral with an imprecisely estimated population ratio; the other is the lack of definitive
37 tools to directly probe iron spin state at high pressures. Two techniques, X-ray emission
38 spectroscopy (XES) and Mössbauer spectroscopy, have been widely used, but their inter-
39 pretation can be ambiguous. The very similar XES spectra [14, 15] and Mössbauer spectra
40 [16–19] have been interpreted in terms of HS-IS and HS-LS crossover in $(\text{Mg,Fe})\text{SiO}_3$ Pv.
41 Plenty of calculations on $(\text{Mg,Fe})\text{SiO}_3$ Pv have been conducted [20–25], but consistency with
42 experiments was not achieved until very recently [26, 27]. Now the spin state in $(\text{Mg,Fe})\text{SiO}_3$
43 Pv is better understood: the observed increase of iron nuclear quadrupole splitting (QS) in
44 Mössbauer spectra results from neither HS-IS nor HS-LS crossover, but from the change in
45 the $3d$ orbital occupancy of the HS iron [27]. As to ferric iron in Pv, possibly more abundant
46 than ferrous iron ($\text{Fe}^{3+} / \sum \text{Fe}$ might be as high as $2/3$) [28, 29], its spin-state crossover has
47 remained unclear, as described below.

48 Previous experiments investigating the iron spin state in aluminum-free MgSiO_3 Pv were
49 focused mostly on ferrous iron [16, 18]. Nevertheless, it was still observed that the low
50 concentration of ferric iron in the sample exhibited an increase in QS with pressure, which

51 suggests a crossover from HS ($S = 5/2$) to LS ($S = 1/2$) state in the pressure range of
 52 30-70 GPa. In contrast, in Al-bearing samples, where ferric iron occupies the dodecahedral
 53 (A) site, the QS remains unchanged up to 100 GPa, which suggests the A-site iron remains
 54 in the HS state [17]. These results indicate that the ferric iron at the octahedral (B) site
 55 undergoes a spin-state crossover. Such a mechanism was recently confirmed by experiments
 56 using $(\text{Mg}_{1-x}\text{Fe}_x)(\text{Si}_{1-x}\text{Fe}_x)\text{O}_3$ Pv ($x = 0.1$) samples: about half of the HS iron changes to
 57 LS state in the 45-60 GPa range while the other half remain in the HS state all the way to
 58 150 GPa [30]. So far, the computational studies on $(\text{Mg}_{1-x}\text{Fe}_x)(\text{Si}_{1-x}\text{Fe}_x)\text{O}_3$ Pv have found
 59 a ground state with HS iron at the A-site and LS iron at the B-site (A-HS; B-LS) and an
 60 A-site HS-LS crossover that leads both A- and B-site iron to a final LS state (A:LS; B-LS)
 61 at high pressures [21, 22]. These predictions are inconsistent with experiments in two ways:
 62 (1) the predicted transition pressure is too high; (2) the predicted HS iron concentration is
 63 too low.

64 To compare with recent experiments [30], we stabilize $(\text{Mg}_{1-x}\text{Fe}_x)(\text{Si}_{1-x}\text{Fe}_x)\text{O}_3$ Pv with
 65 $x = 0.125$ in all possible spin states using a 40-atom supercell shown in Fig. 1. We also
 66 calculate the iron nuclear electric field gradient (EFG) associated with each state, as the nu-
 67 clear hyperfine interaction has proven to be a unique fingerprint to identify the spin states of
 68 transition-metal ions [27, 31]. The atomic structures were fully optimized with damped vari-
 69 able cell shape molecular dynamics [32] implemented in the QUANTUM ESPRESSO code [33],
 70 where the plane-wave pseudopotential method is adopted [34]. These states were also inde-
 71 pendently confirmed via the augmented plane-wave plus local orbitals (APW+lo) method
 72 [35] implemented in the WIEN2k code [36], with which the EFGs were calculated. The EFGs
 73 were converted to QSs with ^{57}Fe nuclear quadrupole moment $Q = 0.16$ [37] and 0.18 barn for
 74 the possible uncertainty. To treat $(\text{Mg}_{1-x}\text{Fe}_x)(\text{Si}_{1-x}\text{Fe}_x)\text{O}_3$ Pv, the density functional the-
 75 ory plus Hubbard U (DFT+ U) method is necessary, as standard DFT exchange-correlation
 76 functionals, the local density approximation (LDA) and generalized gradient approximation
 77 (GGA), sometimes lead to unwanted metallic states (especially at high pressures), in which
 78 the iron spin states are not well defined. Since the Hubbard U of A- and B-site iron in each
 79 spin state is unknown, we have to stabilize the desired spin state with a trial U and then
 80 extract the self-consistent U , referred to as U_{sc} , using the linear response approach [38] in
 81 a recently developed iterative procedure. This procedure is equivalent to, but more efficient

82 than the one published earlier [39], and has been successfully implemented [40]. More details
83 are described in the EPAPS [41].

84 Within DFT+ U , several combinations of iron spin states can be stabilized. The A-site
85 ferric iron can be stabilized in HS, IS, and LS states. The B-site ferric iron can be stabilized
86 not only in LS state, but also in HS state that has not found in previous calculations [21, 22].
87 The spin moments of the A- and B-site iron can be either parallel or anti-parallel. The U_{sc}
88 of ferric iron in Pv, listed in Table I, mainly depends on the iron spin state, slightly depends
89 on the occupied site, and barely depends on pressure and alignment of spin moments.

90 The relative enthalpy (ΔH) of each stabilized state is shown in Fig. 2, where the pre-
91 viously perceived ground state (A-HS; B-LS) [21, 22] is used as a reference. Remarkably,
92 the actual ground state of (Mg,Fe)(Si,Fe)O₃ Pv has HS iron on both sites (A-HS; B-HS),
93 regardless of the choice of exchange-correlation functional (LDA or GGA) and Hubbard U
94 (U_{sc} or 4 eV). These choices do not affect the spin-state crossover either: an HS-LS crossover
95 only occurs in the B-site iron, while the A-site iron remains HS. As expected, the predicted
96 transition pressure (P_T) depends on the exchange-correlation functional and Hubbard U :
97 with LDA+ U_{sc} , $P_T = 41$ GPa; with GGA+ U_{sc} , $P_T = 70$ GPa; with GGA+ U ($U = 4$ eV),
98 $P_T = 29$ GPa. (Coordination complexes also show similar dependence [42, 43].) Notably,
99 the alignment of iron spins (parallel or anti-parallel), barely affects P_T , as shown in Fig. 2(c).
100 The P_T predicted by LDA+ U_{sc} and GGA+ U_{sc} best agree with the P_T observed in Mössbauer
101 spectra, 50-60 GPa [30]. The LDA+ U_{sc} electronic density of states (DOS) of the two relevant
102 states (A-HS; B-HS and A-HS; B-LS) can be found in EPAPS [41].

103 The calculated Qs of ferric iron (A- and B-site) and ferrous iron (A-site) [27] in various
104 spin states, along with the measured Qs [16, 18, 30], are shown in Fig. 3. Clearly, our
105 calculations on ferrous and ferric iron in Pv are consistent with Mössbauer spectra. The
106 HS-LS crossover in the B-site ferric iron also helps to explain the decrease in the XES
107 satellite peak ($K\beta'$) intensity [14, 15]. Interestingly, the QS of ferrous and ferric iron exhibit
108 exactly the opposite trends with respect to the spin moment. This can be understood via
109 their orbital occupancies. The LS ferrous iron, although occupying the A site, is effectively
110 located near the center of a Fe-O octahedron, as it is vertically displaced from the mirror
111 plane [24]. Its six 3d electrons doubly occupy the three orbitals with t_{2g} character and form

112 a charge density with cubic-like shape [24], which barely contributes to the EFG and leads
 113 to a very small QS. The HS ferric iron also has a small EFG (and thus QS), irrespective of
 114 A or B site. This is because its five $3d$ electrons (all spin-up) occupy all $3d$ orbitals, forming
 115 an almost spherically shaped electron charge distribution that leads to a small EFG (and
 116 thus QS). Similarly, the spin-up electrons in HS ferrous and LS ferric iron barely contribute
 117 to EFG, as their charge distributions are nearly spherical and cubic, respectively. It is their
 118 spin-down electrons that contribute to the EFGs and lead to larger QSs. This is why the
 119 spin moments of ferrous and ferric iron appear to affect the QSs in an opposite manner.

120 The LDA+ U_{sc} compression curves and bulk modulus ($K \equiv -VdP/dV$) of $(\text{Mg}_{1-x}\text{Fe}_x)(\text{Si}_{1-x}\text{Fe}_x)\text{O}_3$
 121 Pv ($x = 0.125$) along with the experimental data ($x = 0.1$) [30] are shown in Fig. 4. At
 122 low pressures (< 45 GPa), the experimental data falls on the calculated compression curve
 123 corresponding to the (A-HS; B-HS) state. Starting from ~ 45 GPa, the data points deviate
 124 from the (A-HS; B-HS) curve and then join the (A-HS; B-LS) curve at ~ 60 GPa. Starting
 125 from ~ 100 GPa, the data deviates from the curve again. This, however, is very likely to
 126 result from the questionable accuracy of the Au pressure scale used in the experiment, as
 127 already discussed in the case of $(\text{Mg,Fe})\text{SiO}_3$ Pv [44]. Notice that the observed volume
 128 reduction further confirms the B-site HS-LS crossover, as the previously perceived A-site
 129 HS-LS crossover barely leads to a volume reduction, evident from the compression curves
 130 (A-HS; B-LS and A-LS; B-LS) shown in Fig. 4(a). The B-site spin-state crossover and the
 131 observed volume reduction in the 45-60 GPa range can be qualitatively understood via the
 132 Fe^{3+} electronic configurations and Fe-O distances at A and B sites. With all $3d$ orbitals
 133 occupied, HS iron has spherically-shaped electron charge density and the largest radius
 134 compared with other spin states, favoring longer Fe-O distances. Residing in the large do-
 135 decahedral cage, the A-site iron can easily maintain longer Fe-O distances and thus remain
 136 in HS state. In contrast, the Fe-O octahedron has smaller size and shorter Fe-O distances.
 137 With increasing pressure, the internal octahedron bond lengths can be shortened enough to
 138 induce the HS-LS crossover. Since the $3d$ electrons of the B-site LS iron *only* occupy the
 139 t_{2g} -like orbitals pointing away from oxygen, the associated Fe-O distances are significantly
 140 shorter than those of the HS iron at the same pressure. Therefore, the spin change of the
 141 B-site iron is accompanied by a noticeable octahedral (and thus unit-cell) volume reduction.
 142 Such volume reduction leads to anomalous softening in bulk modulus, as described below.

143 At finite temperatures, the spin-state crossover passes through a mixed-spin (MS) state
144 (namely, HS and LS coexist) within a finite pressure range that increases with temperature.
145 During the crossover, the thermodynamic properties of the MS state exhibit anomalous
146 behavior that may affect mantle properties. One example is the softening in bulk modulus
147 and its effect on the compressional wave velocity, as already seen in ferropericlase [7, 10, 11].
148 To estimate such anomaly in $(\text{Mg,Fe})(\text{Si,Fe})\text{O}_3$ Pv, we employ a thermodynamic model
149 similar to that used in Ref. [10]. Here, we do not include vibrational free energy, as it
150 barely affects the magnitude of the anomaly, slightly increases the transition pressure, and
151 uniformly decreases the bulk modulus, as shown in the case of ferropericlase [10, 11]. Indeed,
152 the calculated $V(P)$ curve of $(\text{Mg,Fe})(\text{Si,Fe})\text{O}_3$ Pv in the MS state (using LDA+ U_{sc}) at room
153 temperature (300 K), shown as the dashed line in Fig. 4(a), exhibits a volume reduction
154 ($\sim 1.2\%$) around the predicted P_T , 41 GPa. This reduction leads to a significant softening
155 in bulk modulus, as shown in Fig. 4(b). The softening is still prominent at 2000 K, the
156 temperature near the top of the lower mantle (~ 660 km deep). Given the abundance of
157 iron-bearing Pv and the possibly high population of ferric iron, this softening may have a
158 noticeable impact on the mantle properties, including possible anomalies in the seismic wave
159 velocities.

160 In summary, with a series of DFT+ U calculations, we have shown that the actual ground
161 state of $(\text{Mg,Fe})(\text{Si,Fe})\text{O}_3$ perovskite has high-spin ferric iron on both A and B sites. It
162 is the B-site ferric iron that undergoes a crossover from high-spin to low-spin state with
163 increasing pressure, while the A-site iron remains in the high-spin state. The calculated
164 quadrupole splittings and the compression curves are consistent with experiments. The
165 volume reduction accompanying the B-site HS-LS crossover leads to a significant softening
166 in bulk modulus, which suggests a possible source of seismic-velocity anomalies in the lower
167 mantle. This work, one more time, demonstrates that the nuclear hyperfine interaction,
168 combined with first-principles calculations, can be a useful tool to identify the spin states of
169 transition-metal ions in solids under high pressures.

170 This work was primarily supported by the MRSEC Program of NSF under Award Number
171 DMR-0212302 and DMR-0819885, and partially supported by EAR-081272, EAR-1047629
172 and ATM-0426757 (VLab). P.B. was supported by the Austrian Science Fund (SFB F41,
173 "ViCoM"). Calculations were performed at the Minnesota Supercomputing Institute (MSI).

-
- 174 [1] *Spin Crossover in Transition Metal Complexes I-III*, Top. Curr. Chem. **233-235**, edited by
175 P. Gülich and H. A. Goodwin (Springer, 2004).
- 176 [2] J. Badro *et al.*, Science **300**, 789 (2003).
- 177 [3] J.-F. Lin *et al.*, Nature **436**, 377 (2005).
- 178 [4] I. Kantor, L. S. Dubrovinsky, and C. A. McCammon, Phys. Rev. B **73**, 100101(R) (2006).
- 179 [5] J.-F. Lin *et al.*, Science **317**, 1740 (2007).
- 180 [6] T. Tsuchiya *et al.*, Phys. Rev. Lett. **96**, 198501 (2006).
- 181 [7] J. Crowhurst *et al.*, Science **319**, 451 (2008).
- 182 [8] A. F. Goncharov *et al.*, Science **312**, 1205 (2006).
- 183 [9] J.-F. Lin *et al.*, Geophys. Res. Lett. **34**, L16305 (2007).
- 184 [10] R. M. Wentzcovitch *et al.*, Proc. Natl. Acad. Sci. **106**, 847 (2009).
- 185 [11] Z. Wu *et al.*, Phys. Rev. B **80**, 014409 (2009).
- 186 [12] J.-F. Lin and T. Tsuchiya, Phys. Earth Planet. In. **170**, 248 (2008), and references therein.
- 187 [13] Han Hsu *et al.*, Rev. Mineral Geochem. **71**, 169 (2010), and references therein.
- 188 [14] J. Badro *et al.*, Science **305**, 383 (2004).
- 189 [15] J. Li *et al.*, Proc. Natl. Acad. Sci. **101**, 14027 (2004).
- 190 [16] J. M. Jackson *et al.*, Am. Mineral. **90**, 199 (2005).
- 191 [17] J. Li *et al.*, Phys. Chem. Minerals. **33**, 575 (2006).
- 192 [18] C. McCammon *et al.*, Nature Geosci. **1**, 684 (2008).
- 193 [19] J.-F. Lin *et al.*, Nature Geosci. **1**, 688 (2008).
- 194 [20] A. M. Hofmeister, Earth Planet. Sci. Lett. **243**, 44 (2006).
- 195 [21] F. Zhang and A. R. Oganov, Earth Planet. Sci. Lett. **249**, 436 (2006).
- 196 [22] S. Stackhouse *et al.*, Earth Planet. Sci. Lett. **253**, 282 (2007).
- 197 [23] A. Bengtson, K. Persson, and D. Morgan, Earth Planet. Sci. Lett. **265**, 535 (2008).
- 198 [24] K. Umemoto *et al.*, Earth Planet. Sci. Lett. **276**, 198 (2008).
- 199 [25] K. Umemoto, H. Hsu, and R. M. Wentzcovitch, Phys. Earth Planet. In. **180**, 209 (2010).
- 200 [26] A. Bengtson *et al.*, Geophys. Res. Lett. **36**, L15301 (2009).
- 201 [27] Han Hsu *et al.*, Earth Planet. Sci. Lett. **294**, 19 (2010).
- 202 [28] C. McCammon, Nature **387**, 694 (1997).

- 203 [29] D. Frost *et al.*, Nature **428**, 409 (2004).
- 204 [30] K. Catalli *et al.*, Earth Planet. Sci. Lett. **289**, 68 (2010).
- 205 [31] Han Hsu *et al.*, Phys. Rev. B **82**, 100406(R) (2010).
- 206 [32] R. M. Wentzcovitch, J. L. Martins, and G. D. Price, Phys. Rev. Lett. **70**, 3947 (1993).
- 207 [33] P. Giannozzi *et al.*, J. Phys.: Condens. Matter **21**, 395502 (2009).
- 208 [34] The pseudopotentials used in this work are the same as those in Ref. [24].
- 209 [35] G. Madsen *et al.*, Phys. Rev. B **64**, 195134 (2001).
- 210 [36] P. Blaha *et al.*, *WIEN2k, An Augmented Plane Wave Plus Local Orbitals Program for Calculating Crystal Properties*, edited by K. Schwarz, Techn. Universität Wien, Vienna (2001).
- 211
- 212 [37] H. M. Petrilli *et al.*, Phys. Rev. B **57**, 14690 (1998).
- 213 [38] M. Cococcioni and S. de Gironcoli, Phys. Rev. B **71**, 035105 (2005).
- 214 [39] H. Kulik *et al.*, Phys. Rev. Lett. **97**, 103001 (2006).
- 215 [40] V. L. Campo Jr and M. Cococcioni, J. Phys.: Condens. Matter **22**, 055602 (2010).
- 216 [41] See EPAPS.
- 217 [42] M. Swart *et al.*, J. Phys. Chem. A **108**, 5479 (2004).
- 218 [43] A. Fouqueau *et al.*, J. Chem. Phys. **122**, 044110 (2005).
- 219 [44] Han Hsu *et al.*, Phys. Earth Planet. In. (2011), doi:10.1016/j.pepi.2010.12.001

220 Table I. U_{sc} , the self-consistent Hubbard U (in eV), of ferric iron on the A and B site in
 221 each spin state.

	A site	B site
HS ($S = 5/2$)	3.7	3.3
IS ($S = 3/2$)	4.6	—
LS ($S = 1/2$)	5.2	4.9

222

Figure Captions

223
224 Fig. 1. (Color online) Atomic structure of $(\text{Mg}_{0.875}\text{Fe}_{0.125})(\text{Si}_{0.875}\text{Fe}_{0.125})\text{O}_3$ Pv, configured
225 with the shortest iron-iron distance, viewing along the [001] direction. Large (orange) and
226 small (green) spheres represent Fe and Mg sites, respectively. Si-O and Fe-O octahedra are
227 shown in opaque (blue) and translucent (orange) colors.

228 Fig. 2. (Color online) Relative enthalpies of $(\text{Mg}_{0.875}\text{Fe}_{0.125})(\text{Si}_{0.875}\text{Fe}_{0.125})\text{O}_3$ Pv in differ-
229 ent spin states obtained using different functionals and Hubbard U . The reference state has
230 HS iron in the A site and LS iron in the B site (A-HS; B-LS). Predicted transition pressures
231 by LDA+ U_{sc} (a), GGA+ U_{sc} (b), and GGA+ U with $U = 4$ eV (c) are 41 and 70, and 29
232 GPa, respectively. Dashed lines in (c) correspond to anti-parallel spins at A- and B-sites.

233 Fig. 3. (Color online) Calculated QSs of (a) ferrous iron [27] and (b) ferric iron in MgSiO_3
234 Pv. Letter A and B in (b) refer to iron-occupying site. Arrows in (c) indicate the measured
235 effect of pressure on QSs [16, 18, 30].

236 Fig. 4. (Color online) Compression curves (a) and bulk modulus (b) of $(\text{Mg}_{1-x}\text{Fe}_x)(\text{Si}_{1-x}\text{Fe}_x)\text{O}_3$
237 Pv computed with LDA+ U_{sc} ($x = 0.125$) and room-temperature measurements ($x = 0.1$)
238 [30]. Both the measured and calculated compression curves exhibit a clear reduction accom-
239 panying with the B-site HS-LS crossover, which leads to a softening in bulk modulus shown
240 in (b).

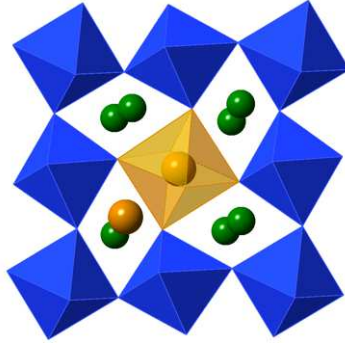


FIG. 1.

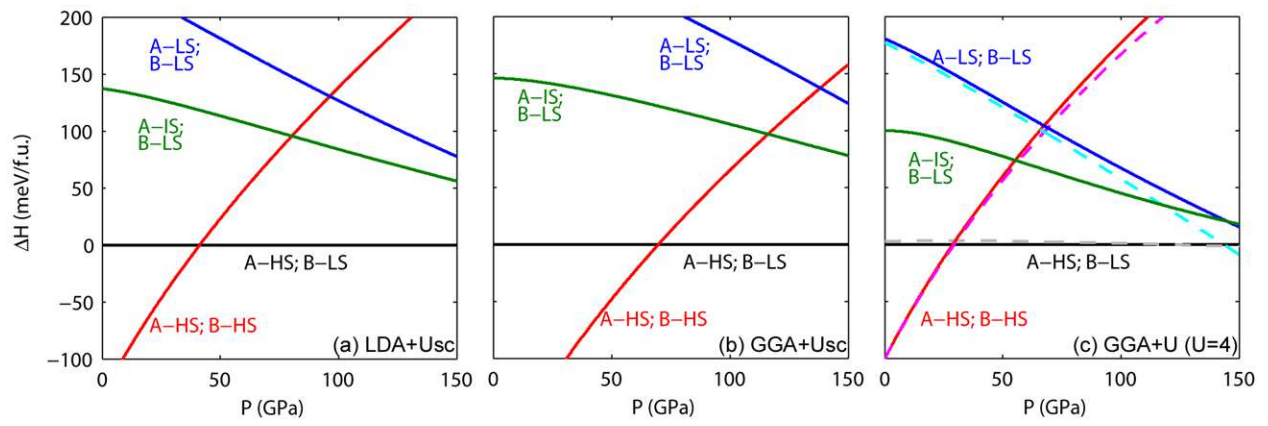


FIG. 2.

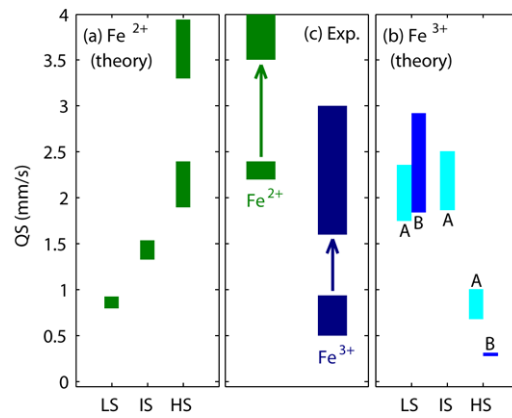


FIG. 3.

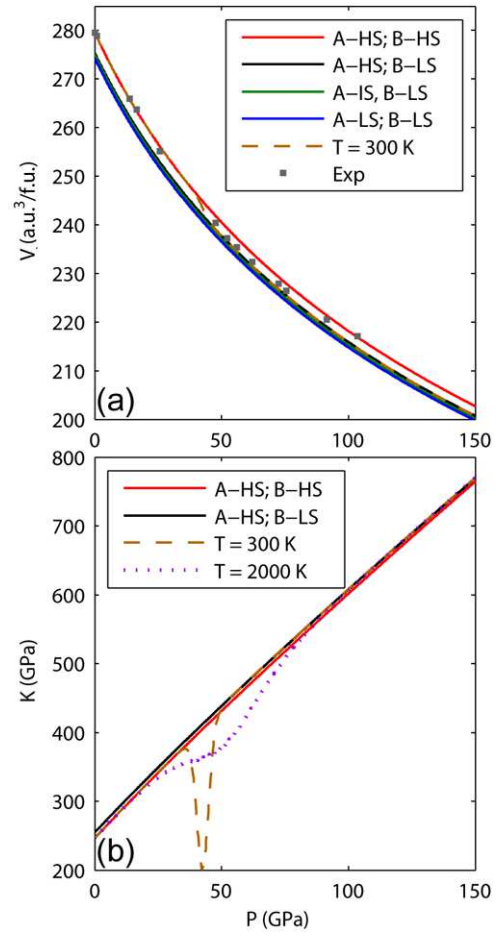


FIG. 4.